

Article

Combined Effects of Thermal Buoyancy, Wind Action, and State of the First-Floor Lobby Entrance on the Pressure Difference in a High-Rise Building

Haiwei Xu *, Lingfeng Su, Wenjuan Lou and Hongyang Shan

College of Civil Engineering and Architecture, Zhejiang University, Hangzhou 310058, China; 11912069@zju.edu.cn (L.S.)

* Correspondence: haiweix@zju.edu.cn

Abstract: The stack effect in high-rise buildings, stemming from an inside/outside temperature difference, may produce a significant pressure difference on the elevator doors, potentially causing elevator malfunctions. This effect can also be influenced by wind action and human behaviors, e.g., opening/closing of building entrances. In this study, a wind tunnel test was conducted to determine the real wind pressure distribution on a high-rise building in northern China. A numerical simulation utilizing the Conjunction of Multizone Infiltration Specialists software (COMIS) was carried out to investigate the pressure difference of elevator doors under the effects of thermal buoyancy, wind action, and opening/closing of the first-floor lobby entrance. An alternative solution of a locally strengthened envelope is proposed and validated for the studied building zone. The study reveals that the opening of the first-floor lobby entrance increases the pressure difference regardless of the environmental conditions, and the increase of wind speed tends to increase the pressure difference in winter but decrease it in summer. The proposed countermeasure combination, involving using revolving doors instead of swing doors, increasing additional partitions, and strengthening the local building envelope, was found to be synergistic and effective in reducing the pressure difference inside the building. The research findings offer practical engineering solutions for mitigating elevator door pressure challenges in high-rise buildings.

Keywords: COMIS simulation; wind tunnel test; pressure difference; high-rise building; pressure mitigation



Citation: Xu, H.; Su, L.; Lou, W.; Shan, H. Combined Effects of Thermal Buoyancy, Wind Action, and State of the First-Floor Lobby Entrance on the Pressure Difference in a High-Rise Building. *Energies* **2024**, *17*, 2117. <https://doi.org/10.3390/en17092117>

Academic Editor: F. Pacheco Torgal

Received: 20 March 2024

Revised: 21 April 2024

Accepted: 21 April 2024

Published: 29 April 2024



Copyright: © 2024 by the authors. Licensee MDPI, Basel, Switzerland. This article is an open access article distributed under the terms and conditions of the Creative Commons Attribution (CC BY) license (<https://creativecommons.org/licenses/by/4.0/>).

1. Introduction

The rapid development of urbanization and construction technology has led to the emergence of high-rise buildings worldwide. A super high-rise building with a frame-core tube structure usually integrates a variety of vertical shafts, such as elevator shafts, duct shafts, and stairwells. These shafts serve as potential pathways for the upward and downward movement of air throughout the high-rise building [1,2]. In winter, the thermal buoyancy caused by the large inside/outside temperature difference will drive warm indoor air to rise through the shafts (e.g., elevator shafts). However, in summer, a reverse airflow process occurs, wherein cool indoor air flows towards the outside of buildings. Such an airflow phenomenon in a high-rise building is called the stack effect [3,4] and it may lead to severe problems in two aspects: one caused by strong flow, e.g., unpleasant noise [5–7] and the propagation of unwanted contaminants [8,9]; the other resulting from excessive pressure difference, e.g., malfunction in opening or closing elevator doors [10,11].

To address these challenges, it is crucial to comprehend the potential influence factors of pressure difference inside buildings, which can be categorized into environmental factors and human behavior factors. Environmental factors primarily include thermal buoyancy induced by an indoor/outdoor temperature difference and wind conditions. The effects of thermal buoyancy and wind on internal pressure difference have been

extensively studied [7–23], with various empirical prediction formulas proposed [14–18]. The studies showed that the vertical distribution of internal pressure difference due to thermal buoyancy is not only determined by the inside/outside temperature difference but also related to the distance from the neutral pressure layer (NPL) [14,19]. However, the horizontal distribution of the internal pressure difference caused by thermal buoyancy and wind action on each floor mainly depends on the arrangement of the compartments (e.g., envelope, internal partitions, vertical shafts, etc.) and their corresponding airtightness [20]. Using the Conjunction of Multizone Infiltration Specialists (COMIS), Khoukhi et al. [21] numerically investigated the combined effects of thermal buoyancy, wind speed, and wind direction on the internal pressure difference and observed significant disturbance in the pressure difference under strong winds. Tan et al. [22] employed a multizone model and computational fluid dynamics (CFD) technology to simulate ventilation of buildings under the combined effects of wind and buoyancy. Based on full-scale experiments, Marcello et al. [23] analyzed the stack and wind effects on single-sided ventilation.

The influence of human behavior on the pressure difference mainly stems from the frequent opening and closing of entrances. For a public or commercial building, there is usually a lobby with a large open area on the first floor. The frequent opening of the entrance creates a main airflow path. Through numerical simulation, Joonghoon et al. [24,25] investigated the effect of opening the lobby doors on the pressure distribution and found that the stack effect became significant when the entrance was open. This suggests that the effects of human behaviors can be coupled with thermal buoyancy, thereby exacerbating excessive pressure problems. In fact, both environmental and human behavior factors can operate simultaneously, and therefore, their combined effects on the pressure difference should be examined. However, few studies have addressed this aspect.

To mitigate pressure difference, considerable countermeasures have been proposed to address stack effect problems, which can be mainly classified into two types: “point to point” methods and global methods. The “point to point” methods aim at changing the distribution of the pressure difference via improvements within specific floors, e.g., implementing revolving doors instead of swing doors on the first floor [25], or increasing horizontal partitions within a floor where the elevators have excessive pressure difference problems [19]. However, such methods have an inherent defect that only the improved positions will be ameliorated and the contribution to the problem mitigation of the overall building is minor, and they may even transfer the pressure difference from one place to another; e.g., applying partitions and revolving doors is effective for pressure mitigation on the target floor with entrances (e.g., first floor), but may increase the pressure difference on other elevator doors. The global method refers to overall improvements of a building, including improving the overall airtightness of the envelope [20], setting vertical segmentation of shafts [26], and using existing HVAC systems [11,27] or elevator cooling systems [28]. However, implementing global methods is quite challenging and expensive, and therefore, is rarely adopted in practice. For example, the elevator shafts have been segmented for architectural purposes in the design stage, such arrangement cannot be changed during occupation. The application of HVAC may have adverse effects on other floors and elevator cooling systems are costly. Moreover, the improper combination of countermeasures can lead to negative interactions and such combined effects will weaker than the sum of their separate effect [20]. Therefore, to solve the over-pressure issue in a more cost-effective way, a comprehensive scheme based on synergistic combinations of different countermeasures needs to be proposed.

By using wind tunnel tests and a COMIS simulation, this study investigates the combined effect of thermal buoyancy, wind action (e.g., speed, direction), and the open/closed state of the first-floor lobby entrance on the vertical and horizontal distribution of pressure difference in a high-rise building. Special attention is paid to the pressure difference acting on three different types of elevators, and their vulnerable floors are identified. A new method for internal pressure mitigation by locally increasing the airtightness of the envelope is proposed and verified. The joint effect of using revolving doors, additional

partitions, and locally strengthened airtightness of the envelope in reducing excessive pressure is explained. This study may provide a feasible and economical solution to the excessive pressure difference problem of high-rise buildings.

2. Description of the Building and Simulation Settings

Overview of the High-Rise Building

The target super high-rise building, with a total height of 360 m (68 floors), shown in the red box of Figure 1, is located in Jinan, northern China, which may experience a large indoor/outdoor temperature difference during the summer and winter seasons and is, therefore, susceptible to the stack effect. The building is enveloped by a curtain wall and has 5 function zones, 6 refuge layers, and 3 lobby floors. Elevator shafts provide the most important vertical airflow paths in this building. There are 3 types of elevators in the building, including short-distance elevators for transportation within respective zones (i.e., A1–A7), long-distance freight elevators (i.e., B1–B2), and shuttle elevators for quick transportation between different zones (i.e., C1–C2), as shown by Figure 2. Most of the elevators will stop at the first floor, where the stack effect is significant and door malfunction is prone to occur due to excessive pressure difference [10,11].



Figure 1. Architectural rendering of the building and the surroundings.

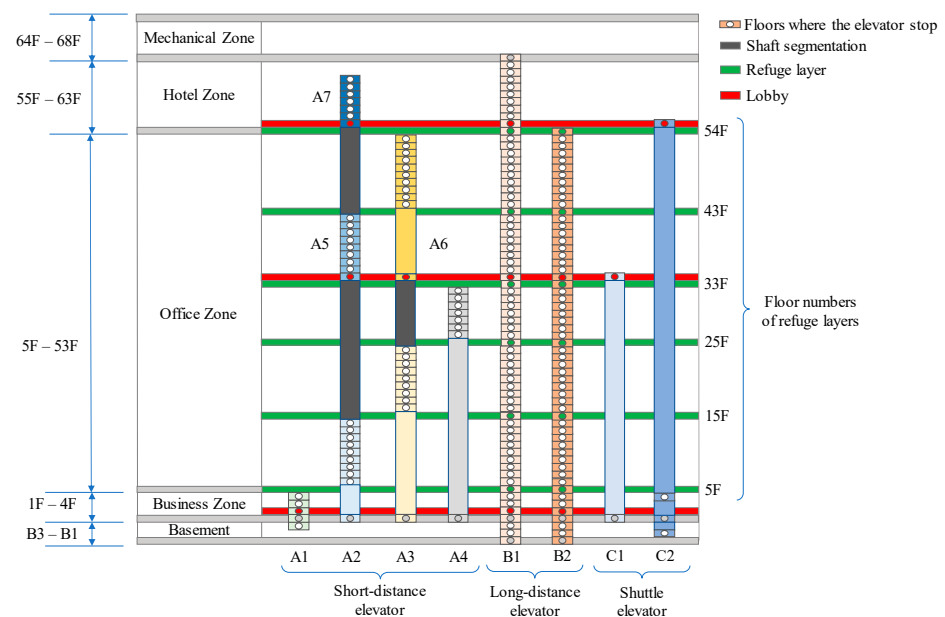


Figure 2. Five zones and the main elevators of the building.

3. Simulation Settings

Wind pressure is one of the main factors influencing the flow pattern inside the building. Therefore, in this study, a wind tunnel test is used to obtain a more accurate wind pressure distribution on the building surface. Based on the measured wind pressure, the COMIS model is employed to investigate the flow pattern and pressure distribution inside the building considering the internal layout. The COMIS model has been extensively validated using measured data [12,15,29–32]. Therefore, the combination of the wind tunnel test and COMIS simulation could provide a reasonable distribution of the pressure difference inside the building.

3.1. The COMIS Model

CONTAMW 2.4, a typical COMIS software, is used for pressure distribution analysis inside the building. COMIS [29] is a network model which simplifies a room or zone as a joint with a constant temperature and contaminant concentration. Each joint is connected with each other joint by openings or gaps to constitute a network. For the building case, a typical office floor plan and the corresponding model are shown in Figure 3. It shows a horizontal airflow pattern where air has to go through the envelope and several partitions before reaching the elevator door (e.g., B1). Therefore, we employed an “envelope–partition–elevator door” structure to describe the horizontal distribution of pressure difference. The pressure difference of the envelope and partitions on the windward, crosswind, and leeward sides were analyzed, as shown by Figure 3.

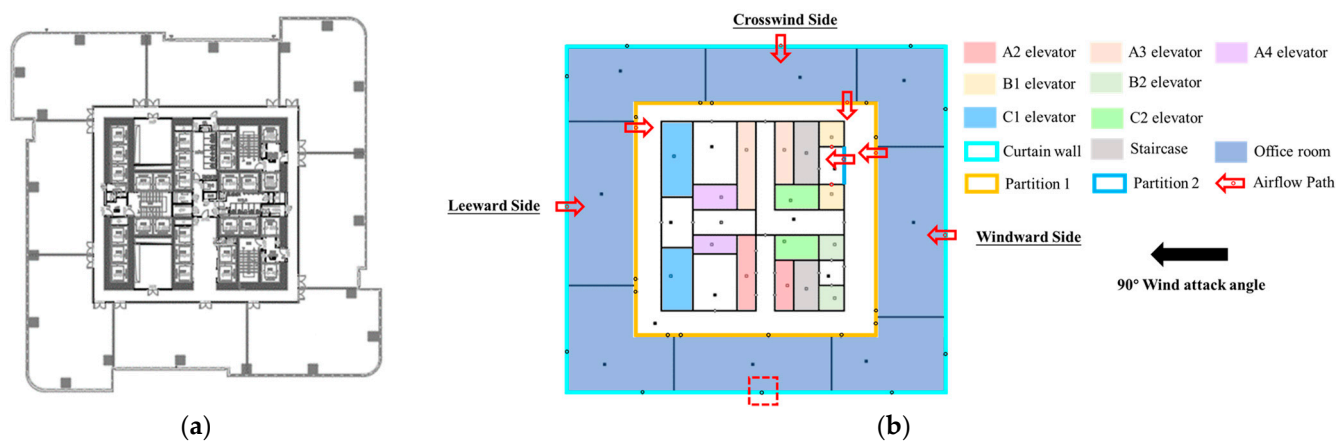


Figure 3. (a) A typical plan of office zone. (b) The corresponding COMIS model.

3.2. Simulation Parameters

3.2.1. Wind Pressure

To obtain the accurate wind pressures for the COMIS simulation, a wind tunnel test was carried out for the building at wind azimuths of 0° – 360° with an interval of 15° (Figure 4a). An acrylonitrile butadiene styrene (ABS)-made model with a geometry scale of 1:400 was investigated in the boundary layer wind tunnel at Zhejiang University, China, as shown by Figure 4b. A boundary layer wind profile representing terrain category B in the Load Code for the Design of Building Structures [33] was simulated at a length scale of 1:400. The experimental mean wind speed at the roof height (i.e., reference height) was 11.1 m/s, and the corresponding wind speed ratio was 1:4.07. Figure 5a compares the normalized experimental wind field with the Chinese specification [34]; good agreement can be observed between the two sets of data. Figure 5b shows that the simulated nondimensional wind velocity spectrum at the roof height was similar to the theoretical Kaimal spectrum. The pressure tap layout on a typical floor is shown in Figure 6a. There are 17 pressure tap layers along the building’s height which are marked as A to P, as shown by Figure 6b. For each wind azimuth, wind pressure signals were recorded at a sampling frequency of 312.5 Hz for a time duration of 32 s. The wind pressure coefficients used for

airflow analysis on an envelope were obtained from the average value of adjacent pressure taps. For example, the wind pressure coefficient for the airflow path through the red dashed box in Figure 3b is the average pressure of measuring points C7 to C10, as illustrated in Figure 6a. Since the pressure taps were not set on each floor, the wind pressure coefficients of unmeasured floors were obtained by the interpolation of two adjacent pressure tap layers (Figure 6b), from Equation (1).

$$C_{pk} = C_{pj} + \frac{C_{pi} - C_{pj}}{\left(\frac{Z_i}{Z_0}\right)^{2\alpha} - \left(\frac{Z_j}{Z_0}\right)^{2\alpha}} \left(\frac{Z_k}{Z_0}\right)^{2\alpha} \tag{1}$$

where C_{pk} is the wind pressure coefficient of the target floor; Z_k is the height of the target floor; C_{pi} is the wind pressure coefficient of the upper measuring point layer, Z_i is the height of the upper measuring point layer; C_{pj} is the wind pressure coefficients of the lower measuring point layer; Z_j is the height of the lower measuring point layer; $Z_0 = 10$ m, and $\alpha = 0.15$, corresponding to terrain category B in the code provisions [33]. For a wind azimuth of 90° , the corresponding results of the windward, leeward, and crosswind wind pressure coefficients of each floor are shown in Figure 7a. During the simulation, the measured pressure coefficients from the wind tunnel test can be input via the “wind pressure profile” function in the CONTAMW software.

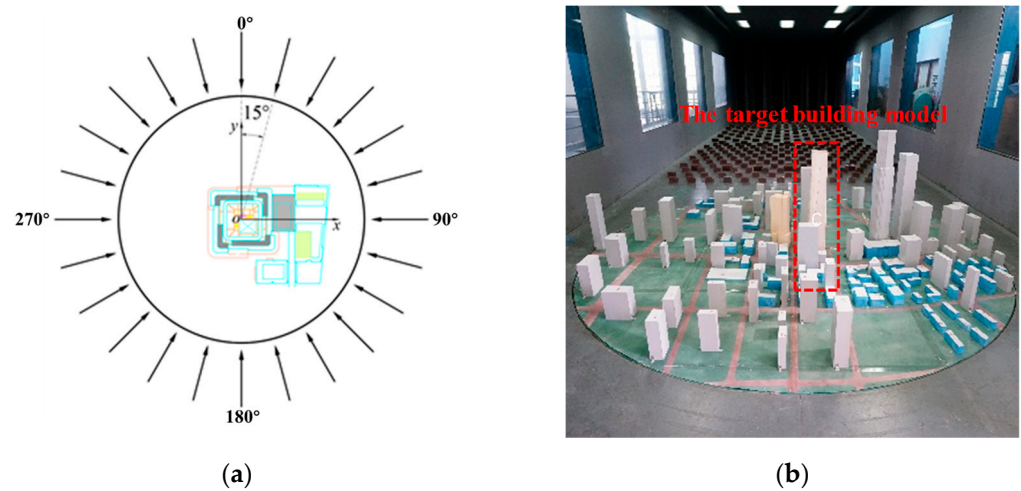


Figure 4. (a) The wind azimuths. (b) The ABS model of the building in the wind tunnel.

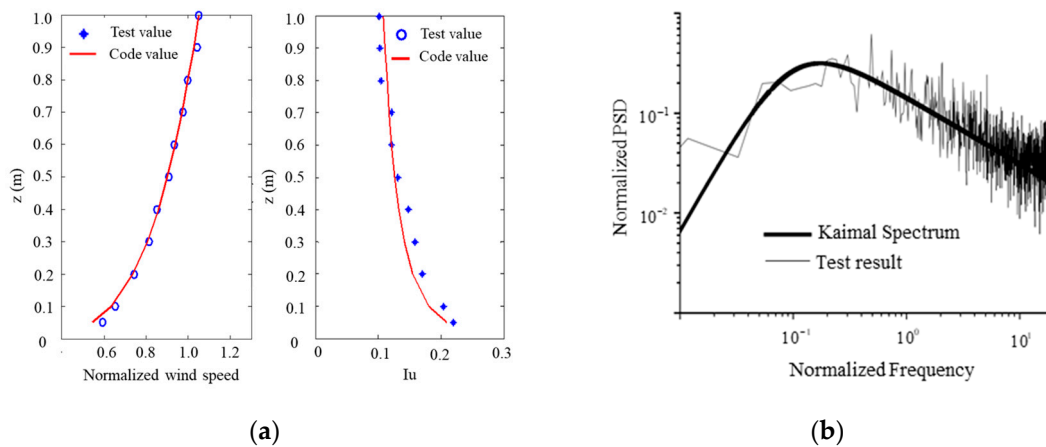


Figure 5. (a) The wind profile and turbulence of the wind field. (b) The PSD of the wind field.

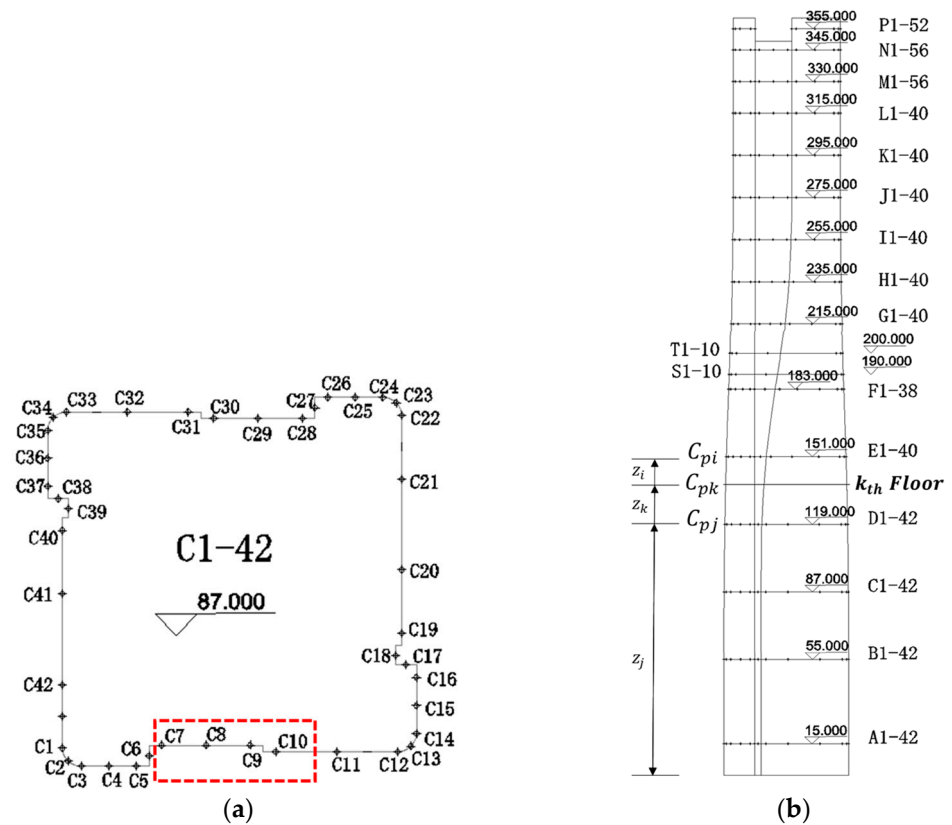


Figure 6. (a) The horizontal arrangement of pressure taps of the marked C tap layer. (b) The vertical distribution of pressure tap layers.

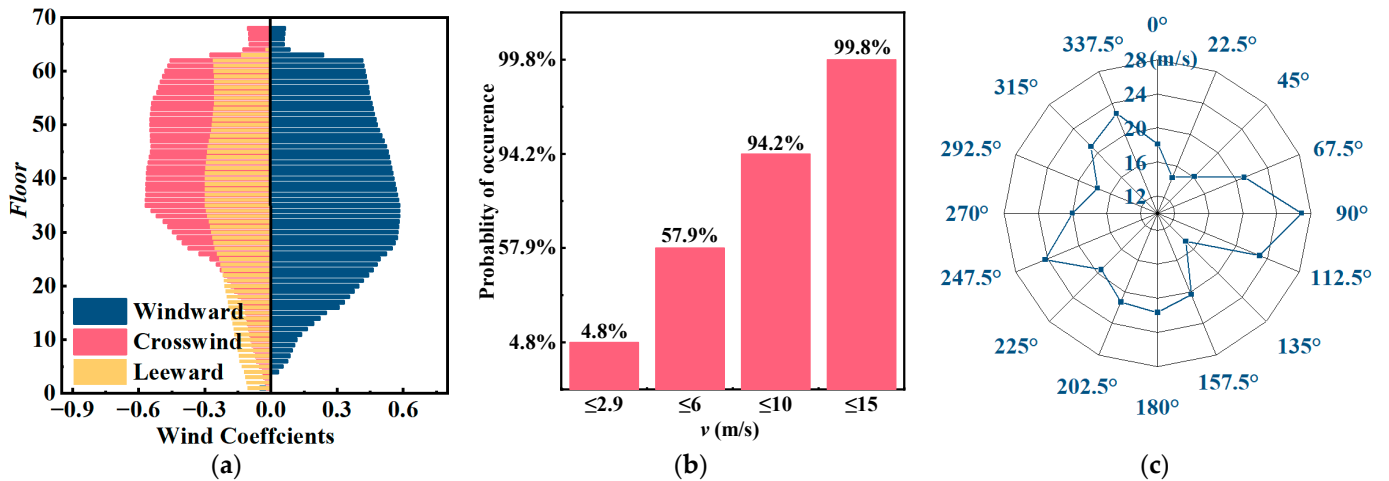


Figure 7. (a) Wind pressure coefficients under 90° in layer unit. (b) Statistical data of wind speed under 90° obtained from the local meteorological station. (c) Wind rose of extreme wind speed under a 50-year return period.

The 10 min averaged wind speed data from 1971 to 2015 is derived from the local meteorological station, and the statistical data and the wind rose of extreme wind speed under a 50-year return period are shown in Figure 7b,c, respectively. Based on the statistical results, the wind speed range under 90° wind azimuth, namely, 0–15 m/s, was used for the COMIS simulation.

3.2.2. Temperature and Airtightness of Structural Components

Considering the large indoor/outdoor temperature difference in summer and winter due to the use of HVAC, the simulation was carried out under the conditions of these two seasons. The indoor and outdoor temperatures for the building can be found in the Chinese specifications [35]; they are $-7.7\text{ }^{\circ}\text{C}$ (outdoor) and $20\text{ }^{\circ}\text{C}$ (indoor) in winter, and $34.7\text{ }^{\circ}\text{C}$ (outdoor) and $24\text{ }^{\circ}\text{C}$ (indoor) in summer, respectively.

The leakage area is adopted to characterize the airtight resistance of compartments, and the corresponding values from different studies are shown in Table 1. For the curtain wall, the air leakage data of level 2 is used for the pressure distribution simulation. Since the studied building is still in the design stage, the relevant simulation parameters are obtained either from code provisions (e.g., GB 50736-2012 [36]) or other previous studies. To investigate the effects of wind action (e.g., speed and direction) and the first-floor entrance status on the distribution of internal pressure difference, 14 simulation cases were conducted in this study and the details are listed in Table 2.

Table 1. The airtightness of building components.

Building Components	Air Leakage Data	Source
Curtain wall	Level 4: $0.5\text{ m}^3/(\text{m}^2\cdot\text{h})$ Level 2: $2\text{ m}^3/(\text{m}^2\cdot\text{h})$	Chinese code [36]
Elevator door	*EqLA ₁₀ : $325\text{ cm}^2/\text{item}$	Ref. [19]
Stairwell door	*EqLA ₇₅ : $120\text{ cm}^2/\text{item}$	
Office door	*EqLA ₁₀ : $200\text{ cm}^2/\text{item}$	Ref. [25]
Revolving door on lobby floor	*EqLA ₁₀ : $10.88\text{ cm}^2/\text{item}$	Ref. [24]
Swing door on lobby floor	*EqLA ₁₀ : $21\text{ cm}^2/\text{item}$	Ref. [37]

* EqLA₇₅: equivalent leakage area at 75 Pa; EqLA₁₀: equivalent leakage area at 10 Pa.

Table 2. Simulation cases.

Effects	Case Number	Outdoor Temperature ($^{\circ}\text{C}$)	Indoor Temperature ($^{\circ}\text{C}$)	Wind Speed (m/s)	Wind Attack Angle	State of the First-Floor Entrance
Wind speed	1	-7.7	20	0	90°	Closed
	2	-7.7	20	6	90°	Closed
	3	-7.7	20	10	90°	Closed
	4	-7.7	20	15	90°	Closed
Wind attack angle	5	-7.7	20	10	0°	Closed
	6	-7.7	20	10	45°	Closed
	7	-7.7	20	10	135°	Closed
	8	-7.7	20	10	180°	Closed
	9	-7.7	20	10	225°	Closed
	10	-7.7	20	10	270°	Closed
	11	-7.7	20	10	315°	Closed
First-floor entrance state	12	-7.7	20	10	90°	Open
Thermal buoyancy	13	34.7	24	10	90°	Closed
	14	34.7	24	10	90°	Open

4. Simulation Results

4.1. The Effect of Wind Speed (Cases 1–4)

The distributions of pressure differences (ΔP) in the envelope, partition, and elevator doors under different approaching wind speeds (cases 1–4) are shown in Figures 8–10, respectively. For the no-wind condition (case 1), it can be observed that the pressure difference on the envelope and elevator doors is relatively small, while that on the partitions is more significant, with large values at the top and bottom of the building due to thermal buoyancy. As the wind speed increases, the wind-induced pressure difference is mainly

borne by the envelope, followed by the partitions, while the ΔP of the elevator doors is rarely affected by the variation in wind speed since most of the air flow is blocked by external curtains and internal partitions.

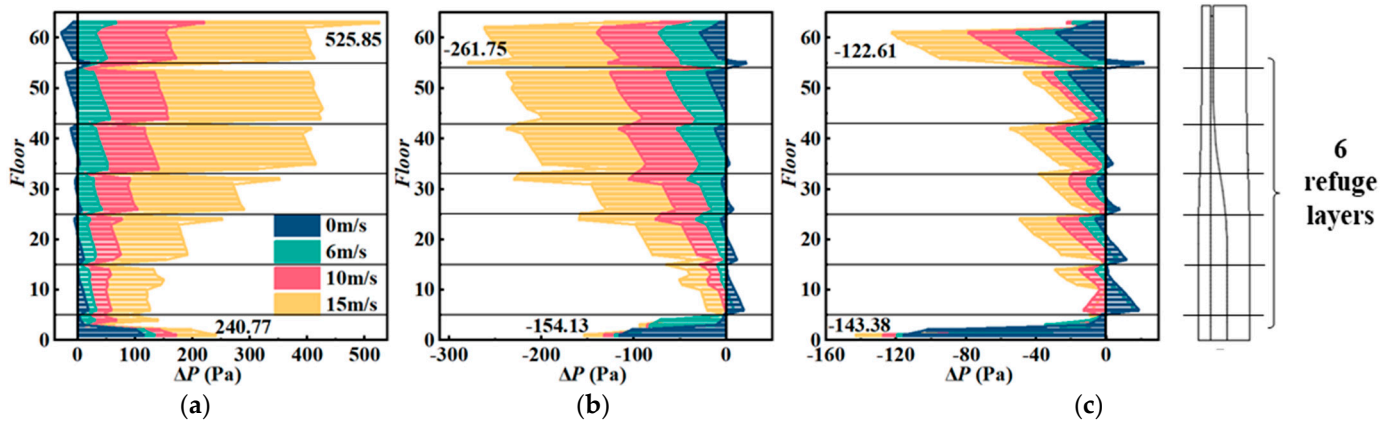


Figure 8. ΔP of envelope under different wind speed. (a) windward side; (b) crosswind side; (c) leeward side.

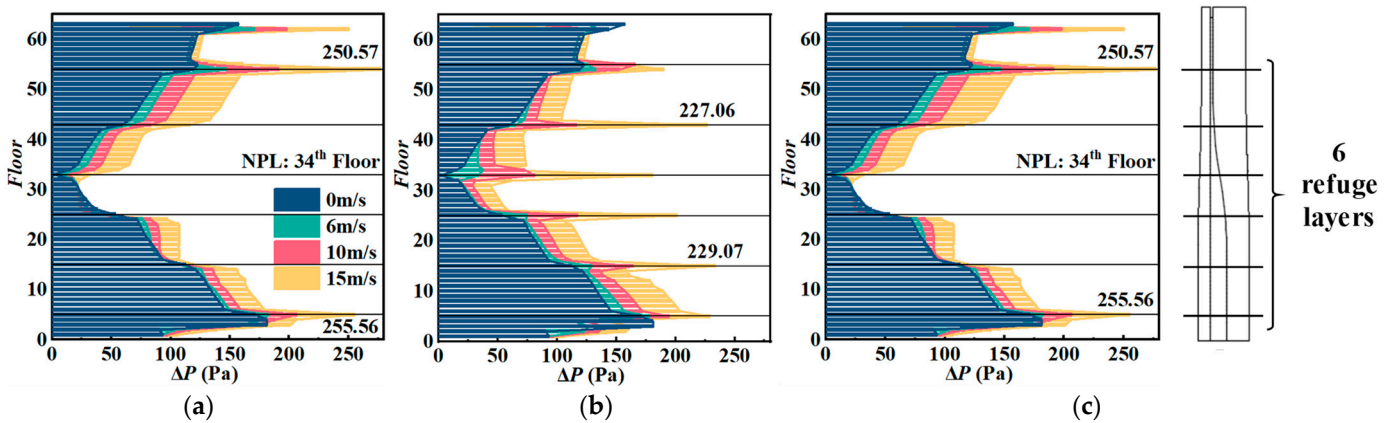


Figure 9. ΔP of partitions under different wind speed. (a) windward side; (b) crosswind side; (c) leeward side.

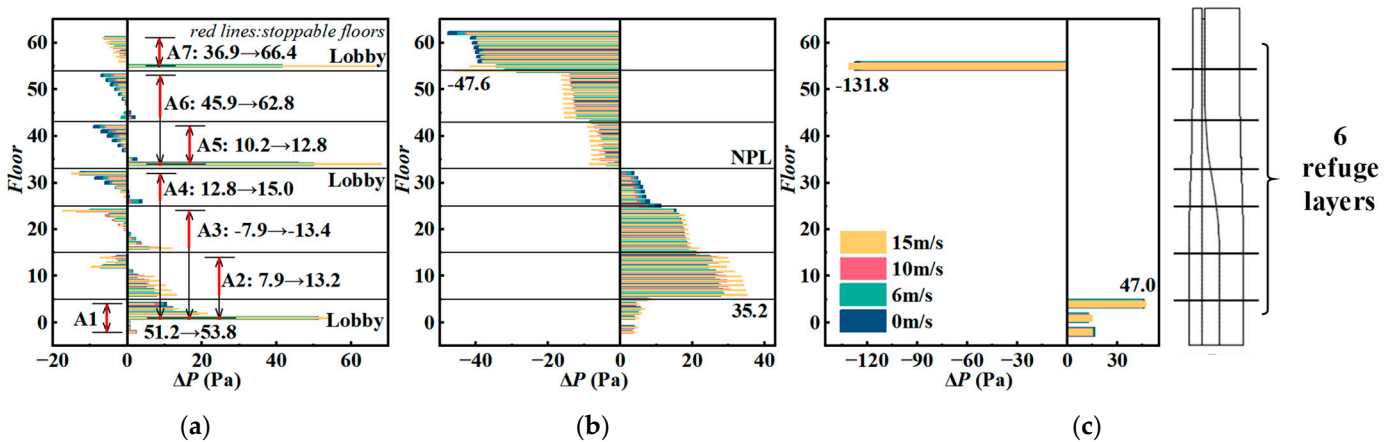


Figure 10. ΔP of elevator doors under different wind speed. (a) seven short-distance elevator doors; (b) B1 long-distance elevator doors; (c) C2 shuttle elevator door.

For the vertical distribution of ΔP on the envelope, Figure 8 shows that the pressure difference is almost linearly distributed between two adjacent refuge layers. With the

increase in wind speed, the ΔP profile is dominated by wind pressure and shows a similar vertical distribution to that of the wind pressure coefficients shown in Figure 8a, which is consistent with the findings in a previous study [21].

For the ΔP distribution of the partitions, as shown in Figure 9, an NPL is observed on the middle-height floor (i.e., 34th floor) when there is no wind, and it disappears when the wind speed increases. In addition, a sharp increase in the ΔP of the partitions appears at most of the refuge layers. This is because the airtightness of the envelope is relatively lower on the refuge layers to satisfy the ventilation requirements of equipment operation, so more wind flow can act directly on the partitions.

Compared to the envelope and partitions, the pressure difference on the elevator doors should be given more attention, as it is the main reason responsible for the malfunction of elevator doors and the noise of elevator shafts. Figure 10 demonstrates the distribution of ΔP for long-distance, short-distance, and shuttle elevator doors along the building height. For short-distance elevators (i.e., A1–A7), ΔP is notable at the lobby floors, namely, the 1st, 34th, and 55th floors, when there is no wind, and it increases apparently with wind speed since the lobbies usually have a large unpartitioned space, leading to less of a barrier between the elevator doors and the external wind. However, for the B1 long-distance elevator used for cargo transportation (Figure 10b), the elevator door is less affected by external wind actions due to the air blocking by partitions. Thus, the vertical distribution for long-distance elevators is mainly determined by the thermal buoyancy and the length of the elevator shaft. Figure 10b also shows that the NPL appears at the middle height of the building, and the floor far away from the NPL bears a larger pressure difference. Comparing Figure 10b,c indicates that a shuttle elevator, which only stops at very limited floors (e.g., shuttle elevator C2 only stops at the 55th floor in the upper part as show in Figure 1), is more sensitive to wind action.

4.2. The Effect of Wind Attack Angle (Cases 3, 5–11)

Since the wind action on a building varies significantly between different approaching directions, it is important to consider the influence of the wind attack angle in the estimation of wind-induced pressure difference. Due to the asymmetry of the building, wind azimuths of 0° – 360° with an interval of 45° were simulated. The effect of the wind attack angle on the ΔP of elevator doors is discussed here and shown in Figure 11.

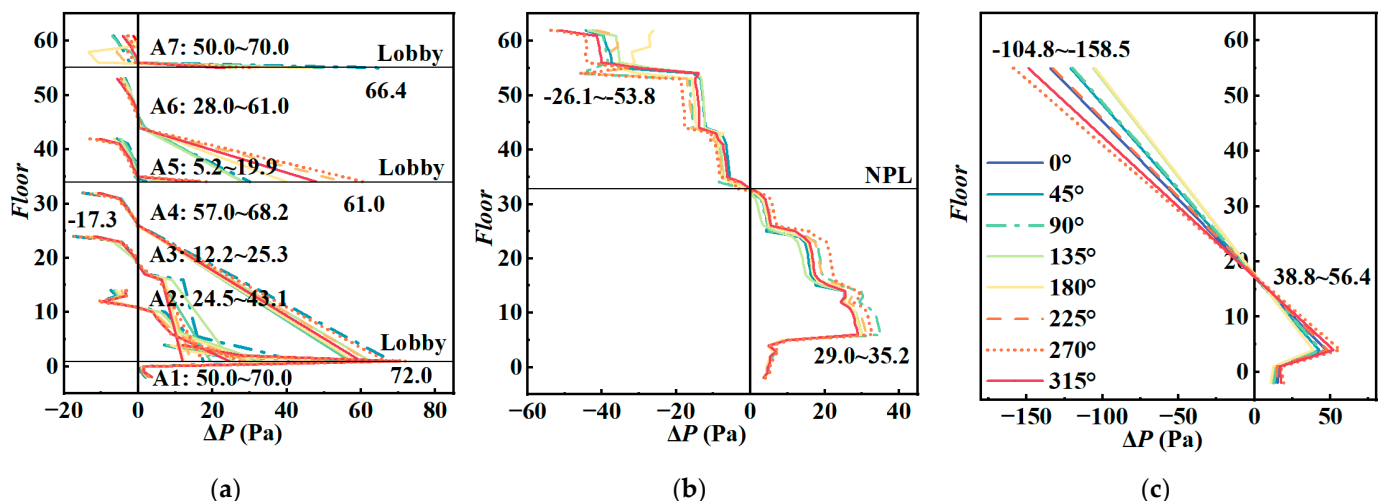


Figure 11. ΔP of elevator doors under different wind direction. (a) seven short-distance elevator doors; (b) B1 long-distance elevator doors; (c) C2 shuttle elevator door.

It can be observed that the wind attack angle has a significant effect on the distribution of ΔP , and the largest ΔP values of different types of elevators mainly appear at wind attack angles of 90° and 270° . For short-distance elevators, the largest pressure difference can be found on the three lobby floors, which are also sensitive to the wind direction. For the

shuttle elevator C2, the largest pressure difference appears on the highest floor on which it can stop, and varies significantly from -104.8 Pa to -158.5 Pa with the change in wind attack angle. Compared to the short-distance elevators and shuttle elevators, the influence is much less for the long-distance elevators.

4.3. The Effect of Open/Closed States of the First-Floor Entrance (Case 12)

Figures 12–14 show the influence of the open/closed states of the first-floor entrance on the ΔP distribution. It shows that the overall profiles of ΔP for the envelope, partition, and elevator remain almost the same before and after the entrance door opens, except for the several low-level floors near the first one, indicating a limited local effect caused by the opening of the first-floor entrance.

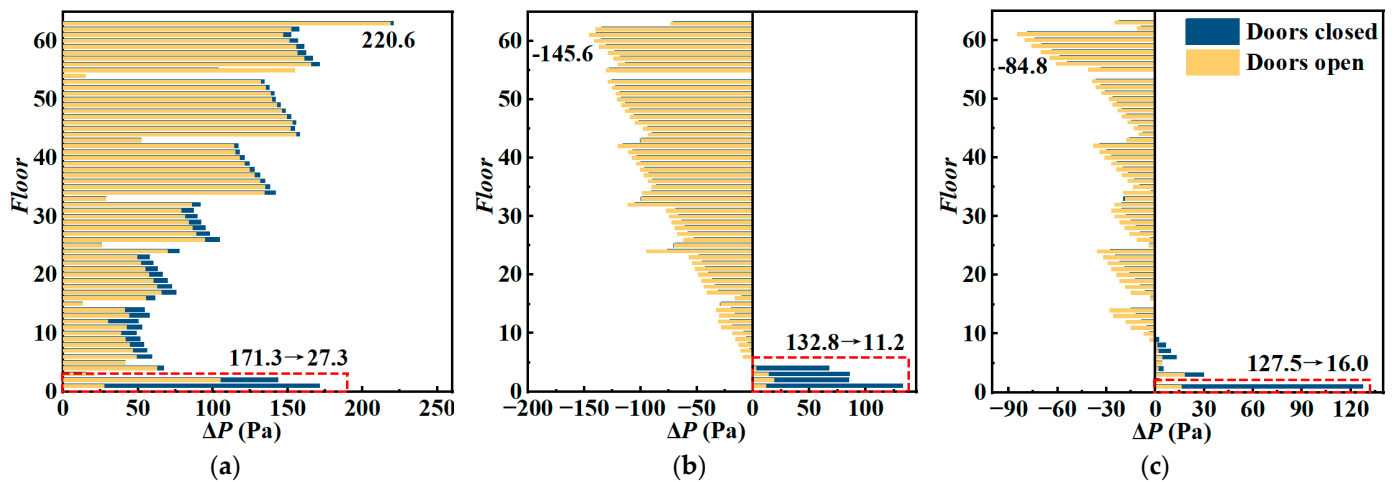


Figure 12. ΔP of envelope when the first-floor entrance is opening. (a) windward side; (b) crosswind side; (c) leeward side.

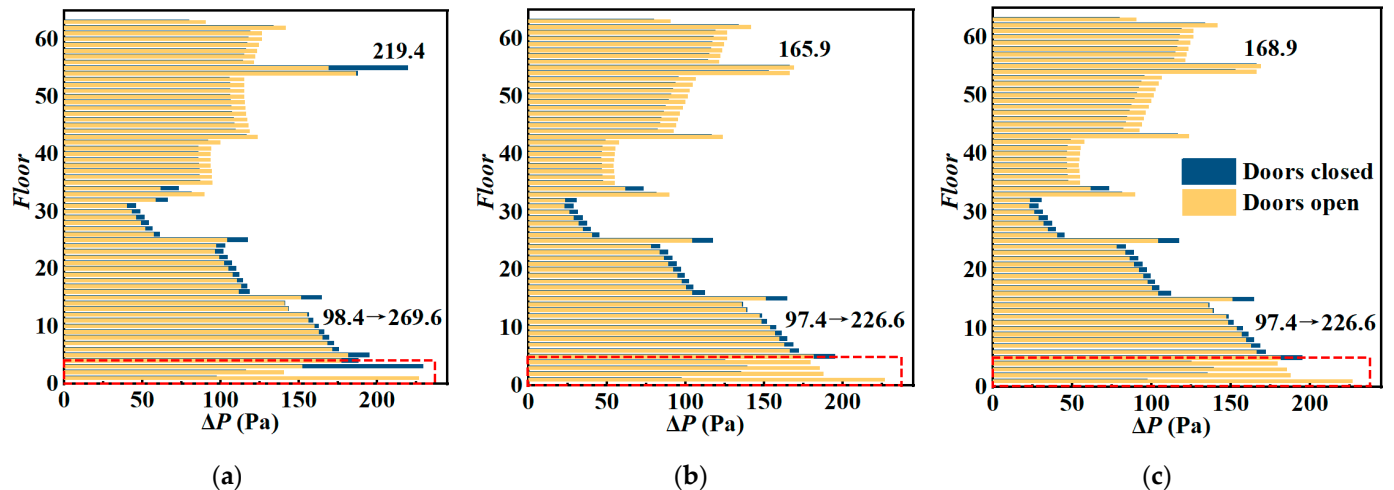


Figure 13. ΔP of partitions when the first-floor entrance is opening. (a) windward side; (b) crosswind side; (c) leeward side.

For the envelope, Figure 12 shows that the ΔP of the first-floor is significantly decreased on all sides. The largest decrease in ΔP is on the windward side, followed by the crosswind and leeward sides. However, for the partitions in Figure 13, an opposite trend can be observed for ΔP on the first-floor, where it increases significantly to over 200 Pa (more than doubled) after the door is opened.

For elevator doors, the effect of entrance opening for short-distance elevators is significant on the lobby floors, as shown in Figure 14. For long-distance elevator B1, such an

effect is insignificant. However, for the shuttle elevator C2, when the entrance door on the first floor opens, both the positive ΔP on the first-floor and the negative ΔP increased remarkably, which results in pressure difference problems on both the lower and higher parts of the elevator. It also means that the opening of the first-floor entrance can have an overall effect on the shuttle elevator.

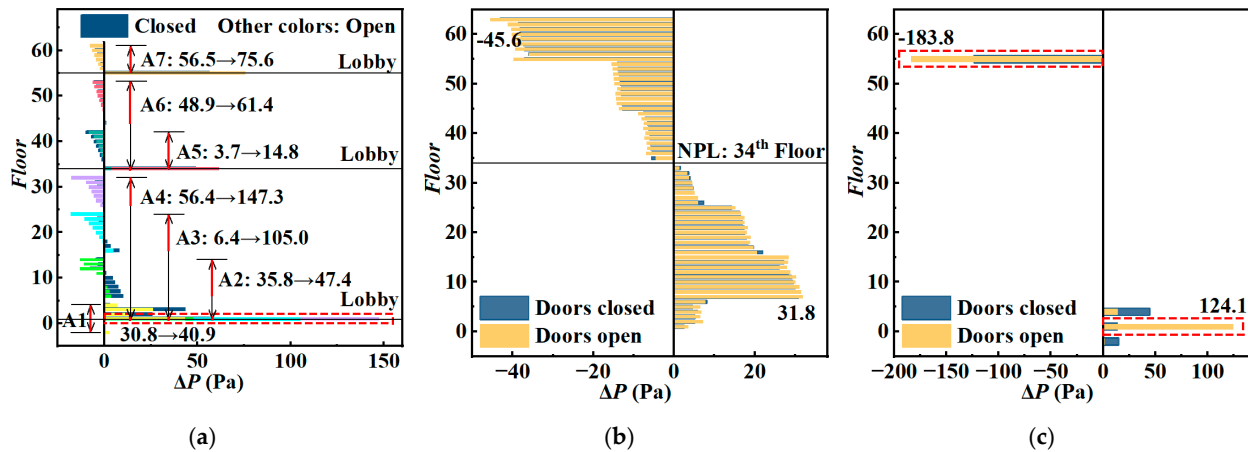


Figure 14. ΔP of elevator doors when the first-floor entrance is opening. (a) seven short-distance elevator doors; (b) B1 long-distance elevator doors; (c) C2 shuttle elevator door.

4.4. The Combined Effect of Wind Speed and the Opening of the First-Floor Lobby Entrance under Different Temperature Environments (Cases 3, 12–14)

Based on two different temperature environments, namely, winter and summer conditions, Figure 15 shows the combined effects of wind speed and the opening of the first-floor lobby entrance on the pressure difference of the elevator doors. The elevators with maximum pressure differences (ΔP_{max}) occurring on the first-floor (i.e., A3, A4, and C1) are chosen for study at a wind direction of 90° . It can be found that opening the entrance will enlarge the pressure difference no matter whether it is winter or summer. However, wind action may exert opposite effects on the pressure difference in winter and summer; there is an increasing and decreasing tendency in the pressure difference with increases in wind speed in winter and summer, respectively. This is because in winter the airflow induced by the thermal buoyancy and wind are both upward, and thus, exacerbate the pressure acting on the first-floor elevator door, while in summer the inverse thermal buoyancy effect (from building interior to external environment) will neutralize the incoming wind flow through the opening entrance or building leakage, and thus, reduce the pressure difference.

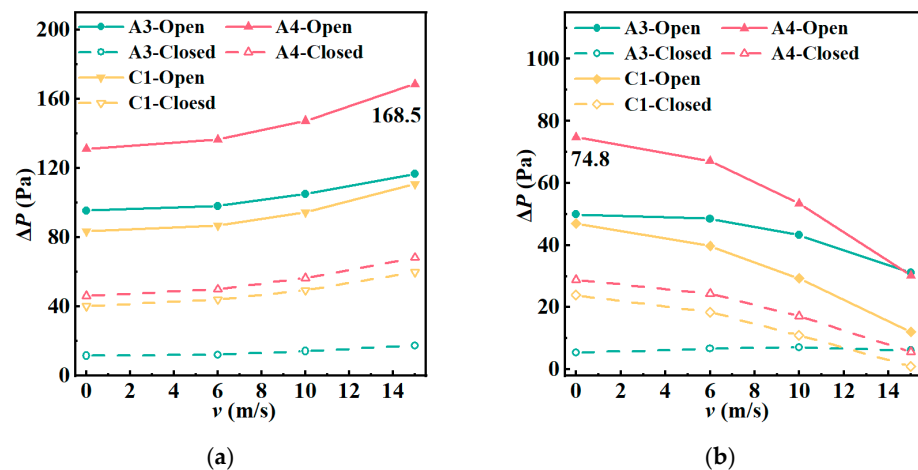


Figure 15. (a) ΔP_{max} of elevator doors occurring on the first-floor in winter; (b) ΔP_{max} of elevator doors occurring on the first-floor in summer.

Table 3 further lists the ΔP_{max} value of all the elevators under all cases listed in Table 2, along with the corresponding floor number and the main causes. According to previous studies [19,36,38–40], the pressure difference of elevator doors should be less than 50 Pa for their proper operation, thus this value is chosen as the standard of whether the elevator malfunctions or not. Table 3 shows that the ΔP_{max} floors basically appear at the entrance floor (i.e., 1st floor), lobby floors (i.e., 34th and 55th floor) and the top floor of elevator (i.e., 63rd floor) and that thermal buoyancy is one of the main reasons for exceeding the 50 Pa standard for all types of elevators. But there are other main factors for different elevator types. For short-distance elevators, opening first-floor lobby entrance and wind action are other main reasons for elevators A1–A4 and elevators A6–A7, respectively. For long-distance elevators and shuttle elevators, the other main reasons are the wind attack angle and opening first-floor lobby entrance, respectively.

Table 3. The ΔP_{max} values and the corresponding floors and dominant factors of all discussed elevators.

Type	Short-Distance Elevator					Long-Distance Elevator				Shuttle Elevator	
Number	A1	A2	A3	A4	A5	A6	A7	B1	B2	C1	C2
ΔP_{max} (Pa)	70.0	47.4	105.0	147.3	14.8	61.4	75.6	−53.8	−53.1	−123.5	−183.8
Exceed 50 Pa	Yes	No	Yes	Yes	No	Yes	Yes	Yes	Yes	Yes	Yes
Floor of ΔP_{max}	1st	1st	1st	1st	34th	34th	55th	63rd, 54th	1st	1st	55th
Main reasons	Thermal buoyancy Opening first-floor lobby entrance /					Wind action		Thermal buoyancy Wind attack angle		Thermal buoyancy Opening first-floor lobby entrance	

5. Countermeasures for Excessive Pressure Difference

5.1. A New Method: Locally Strengthened Airtightness of Envelope

Increasing the airtightness of the envelope has proven to be an effective method of reducing all indoor pressure differences, as it increases the whole pressure-bearing capacity of the envelope. Although improving the overall airtightness is very expensive and impractical, strengthening airtightness in local areas of a building is still an option for certain floors suffering from an excessive pressure problem. Table 3 demonstrates that the ΔP_{max} of elevator doors is prone to appear at a few floors, e.g., the 1st floor, 34th floor, 55th floor and 63rd floor, which are the main focus of pressure mitigation. Thus, a locally strengthened envelope may be applied in these local areas.

To verify the validity of the proposed method, we select the business zone and hotel zone (i.e., 1st to 4th floor and 55th to 63rd floor) for study. The airtightness of the envelope for these floors is strengthened from level 2 to level 4 according to the specification [35]. Based on the parameter conditions of case 5, the profiles of ΔP before and after local and overall enhancement of airtightness are compared in Figures 16–18.

Figures 16–18 show that the pressure difference in strengthened zones marked by the red boxes is consistent with the overall enhanced profile (level 4), while that in un-strengthened zones remains almost the same as the profile of level 2, which implies that the effect of locally strengthened airtightness is only limited within the target zones. However, such an effect could be different for the envelope and partitions and elevator doors. For the envelope (Figure 16), it can be observed that ΔP at most of the floors increases after enhancement of the envelope, indicating that the envelope bears most of the wind action. In this case, the pressure difference on the partitions and elevator doors will be reduced significantly, as corroborated by Figures 17 and 18. The mechanism of applying a locally strengthened curtain is to redistribute pressure difference between the curtain and the elevator doors. This could be an effective solution for local floors where elevators have problems of excessive pressure difference but where it is unsuitable to set additional partitions (e.g., lobby). Since high-rise buildings are usually enveloped by a curtain wall [37], a locally improved airtightness envelope can be conveniently achieved by identifying and better sealing off the air paths of the curtain wall [38], and such local improvement (i.e., from level 2 to level 4 for envelope airtightness) is more economical than overall airtightness strengthening of the whole building [20].

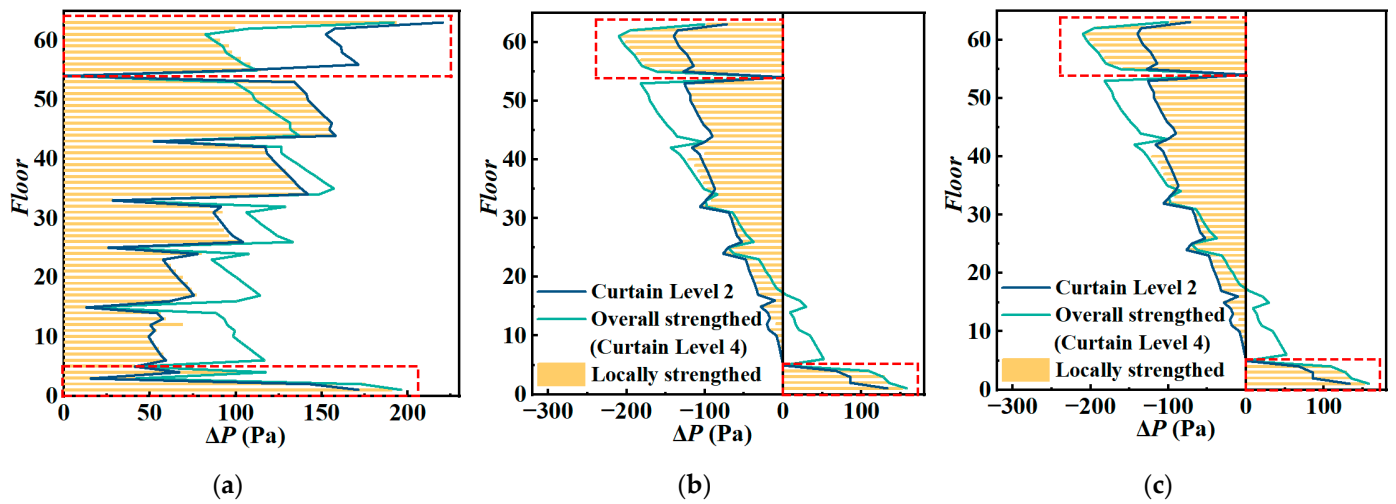


Figure 16. ΔP of envelope under different airtightness of envelope. (a) windward side; (b) crosswind side; (c) leeward side.

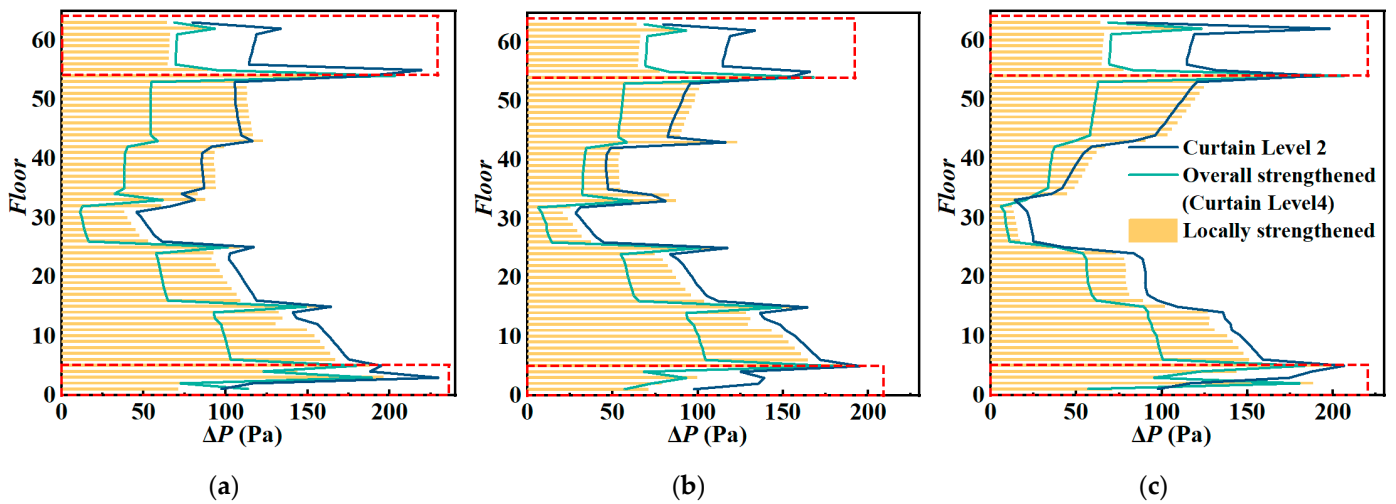


Figure 17. ΔP of partitions under different airtightness of envelope. (a) windward side; (b) crosswind side; (c) leeward side.

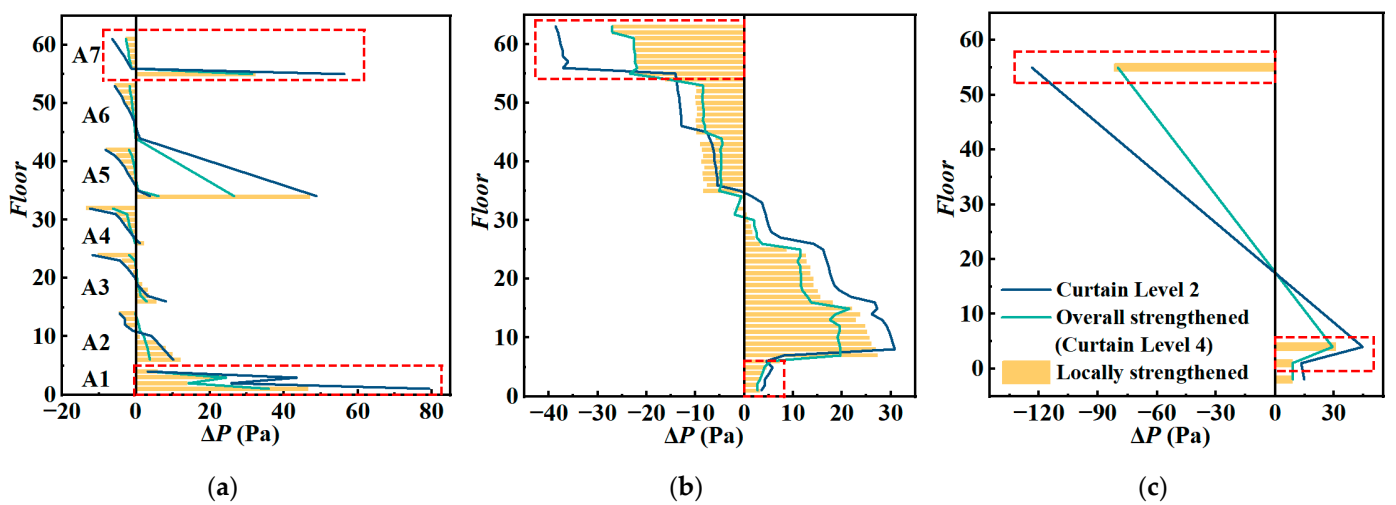


Figure 18. ΔP of elevator doors under different airtightness of envelope. (a) seven short-distance elevator doors; (b) B1 long-distance elevator doors; (c) C2 shuttle elevator door.

5.2. The Synergistic Effect of a Comprehensive Countermeasure Scheme

In this section, the effect and synergy of a comprehensive countermeasure scheme, namely, using revolving doors to replace swing doors for the first-floor entrance, applying additional partitions, and strengthening the local building envelope, is investigated.

Firstly, swing doors on the first floor are replaced with revolving doors to maintain the uniformity of the envelope airtightness. For elevator doors with excessive pressure, the simplest way should be applying a partition closely in front of the door, which will effectively relieve pressure difference on the elevator door. According to the results in Table 3, the additional partitions are set as shown in Figure 19. The locally strengthened airtightness zones of the envelope are the same as in Section 5.1 (i.e., 1st to 4th floor and 55th to 63rd floor). Typical elevators covering all three types and different floors are considered herein, including A4 (floor 1 to floor 32), A6 (floor 34 to floor 53), A7 (floor 55 to floor 61), and shuttle elevator C2 (floor B2 to floor 55). The initial ΔP_{max} of these four elevators all exceed 50 Pa, which needs to be mitigated.

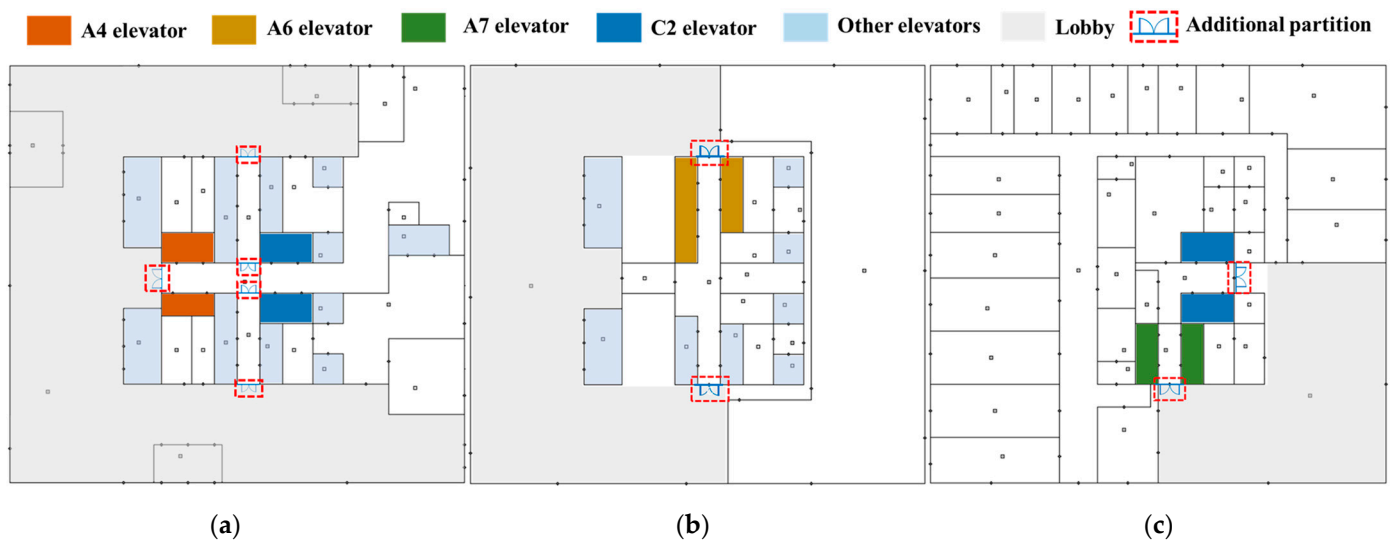


Figure 19. The arrangement of additional partitions: (a) the 1st floor; (b) the 34th floor; (c) the 55th floor.

The three countermeasures and their different combinations were applied for two dangerous wind directions (i.e., 90° and 270°), and the results of ΔP_{max} before and after applying countermeasures are plotted in Figures 20 and 21. They both show an obvious downward trend with the increase in countermeasures. When the revolving doors are implemented, the ΔP_{max} of all of the selected elevators decreases; with the most significant decreases for elevators A4 and C2, which stop at the first floor. This phenomenon is similar to the findings of previous studies [24]. When the measure of a revolving door is combined with either a locally strengthened envelope or additional partitions, a more significant reduction in ΔP can be observed for elevators A7 and C2. For elevators A7 and C2, whose doors are all within the curtain-strengthened zone, the effect of the locally strengthened envelope is similar to that of additional partitions, indicating that locally strengthening the envelope can be a good substitute for additional partitions. However, for elevators A4 and A6, whose doors are not all within the strengthened zone, the contribution of locally enhancing the envelope's airtightness is much weaker. This can be attributed to the unevenly distributed airtightness along the height. Thus, for elevators whose doors are not all within the strengthened zone, these two measures are interchangeable.

However, there are still some cases where the pressure difference is above 50 Pa (e.g., elevator C2), even after applying two countermeasures together. Therefore, all three countermeasures were used, leading to all the ΔP s of the elevator doors being below the 50 Pa standard, which demonstrates the favorable synergistic interaction of the three

countermeasures. Apart from this, the synergistic effect is insignificant for the elevators whose doors are not all within the strengthened zone (i.e., A4 and A6). The application of synergistic countermeasures may change the location of the ΔP_{max} of elevators. For example, for the A4 elevator at a 90° wind azimuth, when three countermeasures work simultaneously, the ΔP_{max} floor changes from the 1st floor to the 32nd floor. Therefore, the combination of different countermeasures should be carried out carefully to obtain a reasonable scheme.

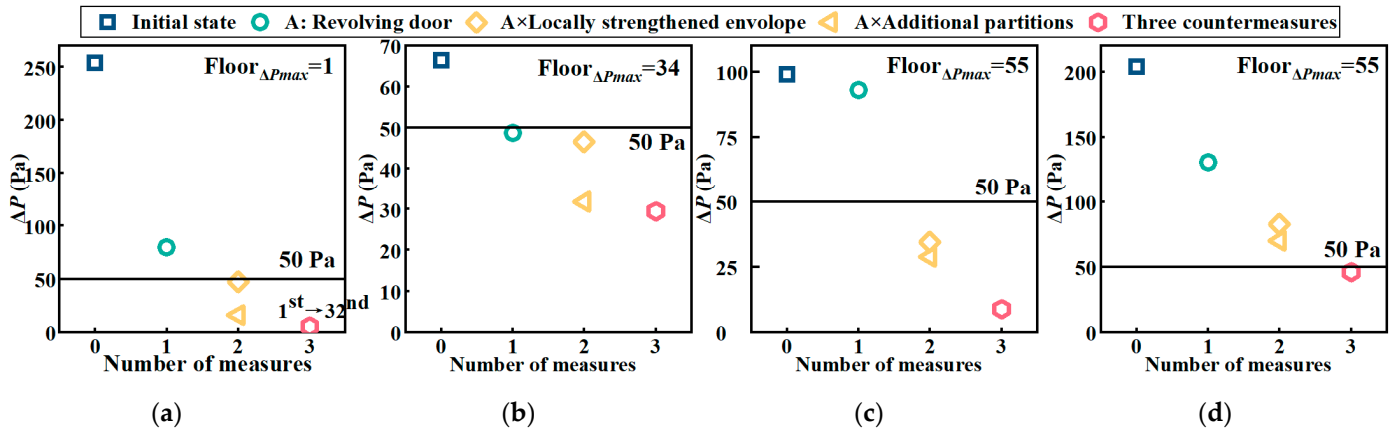


Figure 20. The synergistic interaction of three countermeasures at wind azimuths of 90° : (a) A4 elevator; (b) A6 elevator; (c) A7 elevator; (d) C2 elevator.

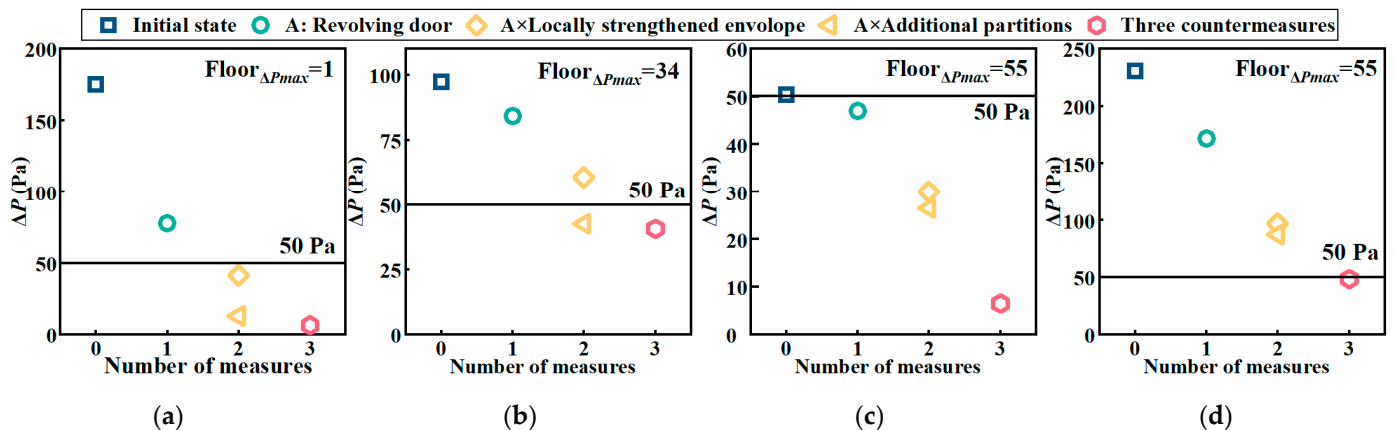


Figure 21. The synergistic interaction of three countermeasures at wind azimuths of 270° : (a) A4 elevator; (b) A6 elevator; (c) A7 elevator; (d) C2 elevator.

6. Conclusions

This study carried out wind tunnel tests and COMIS simulations to investigate the combined effect of thermal buoyancy, wind action, and the open/closed state of the first-floor lobby entrance on the pressure difference in a high-rise building. And the effects of a new mitigation method and a synergistic countermeasure scheme to relieve the over-pressure on elevator doors were presented. The main conclusions are:

(1) The wind-induced pressure difference is mainly borne by the envelope, followed by the partitions, and elevator doors. An increase in wind speed will increase the pressure difference of elevator doors in winter, but reduce it in summer, thus alleviating the stack effect. Under different wind attack angles, the pressure difference inside the building varies significantly and could exceed the threshold of normal use even under the same wind speed.

(2) The opening of the first-floor entrance increases the pressure difference of the elevator door, especially for the elevators that stop at the first-floor and have no partitions in the airflow path. For short-distance elevators, the effect of opening lobby entrance is

limited within nearby floors, but for shuttle elevators, a significant pressure increase can be observed on the top-level floor.

(3) A locally strengthened envelope can remarkably reduce the elevator door pressure difference on the targeted floors, but its effect on the unstrengthened floors is minor. Therefore, it can be a good countermeasure for the local floors where multiple elevators are under excessive pressure difference but where it is unsuitable to set additional partitions.

(4) The pressure mitigation effect becomes more apparent with the increase in the number of countermeasures, showing good synergy. But for the elevators whose doors are not all within the strengthened envelope zones (e.g., elevators A4 and A6), the combination of two methods (e.g., revolving doors and local strengthened envelope, revolving doors and additional partitions) can achieve a similar mitigation effect to that of all of the methods combined (i.e., revolving doors, local strengthened envelope, and additional partitions). Therefore, the combination of different countermeasures should be selected carefully to achieve cost-effective pressure mitigation.

Author Contributions: All authors contributed to the study conception and design. Material preparation was performed by H.S., data collection and analysis were performed by L.S., H.X. and W.L. The first draft of the manuscript was written by L.S. and revised by H.X. All authors commented on previous versions of the manuscript. All authors have read and agreed to the published version of the manuscript.

Funding: This research was funded by the National Natural Science Foundation of China (Grant No. 51978614).

Data Availability Statement: Dataset available on request from the authors.

Conflicts of Interest: The authors declare no conflicts of interest.

References

1. Doosam, S.; Sungmin, Y.; Chanwoul, J.; Joowook, K.; Hyunwoo, L. Heat, vapor, and CO₂ transportation caused by airflow in high-rise residential buildings. *Build. Environ.* **2019**, *160*, 106176.
2. Sowoo, P.; Yun, C.; Hyunwoo, L.; Doosam, S. Analysis of vertical movement of particulate matter due to the stack effect in high-rise buildings. *Atmos. Environ.* **2022**, *279*, 119113.
3. Tamura, G.T. *Smoke Movement and Control in High-Rise Buildings*; National Fire Protection Association: Boston, MA, USA, 1994.
4. Khoukhi, M.; Asma, A.M. Stack Pressure and Airflow Movement in High and Medium Rise buildings. *Energy Procedia* **2011**, *6*, 422–431. [[CrossRef](#)]
5. Doosam, S.; Hyunwoo, L.; Joonghoon, L.; Jungmin, S. Application of the mechanical ventilation in elevator shaft space to mitigate stack effect under operation stage in high-rise buildings. *Indoor Built Environ.* **2014**, *23*, 81–91.
6. Antony, W.; Ruba, S. *Guide to Natural Ventilation in High Rise Office Buildings*, 1st ed.; Routledge: London, UK, 2012; p. 184.
7. Ai, Z.T.; Mak, C.M.; Cui, D.J. On-site measurements of ventilation performance and indoor air quality in naturally ventilated high-rise residential buildings in Hong Kong. *Indoor Built Environ.* **2015**, *24*, 214–224. [[CrossRef](#)]
8. Hyesoo, S.; Byungseon Sean, K.; Taeyeon, K.; Jeonghee, L. Influence analysis of stack effect on odor dispersion from unit to core in the high-rise residential buildings. *Proc. Build. Simul.* **2007**, 1062–1068.
9. Taesub, L.; Jinkyun, C.; Byungseon, S.K. Predictions and measurements of the stack effect on indoor airborne virus transmission in a high-rise hospital building. *Build. Environ.* **2011**, *46*, 2413–2424.
10. Sergey, M.; Stefano, C. Stack effect in high-rise buildings: A review. *Int. J. High-Rise Build.* **2016**, *5*, 327–338.
11. Jung-yeon, Y.; Kyoo-dong, S.; Dong-woo, C. Resolving stack effect problems in a high-rise office building by mechanical pressurization. *Sustainability* **2017**, *9*, 1731.
12. Yoon, S.; Song, D.; Kim, J.; Lim, H. Stack-driven infiltration and heating load differences by floor in high-rise residential buildings. *Build. Environ.* **2019**, *157*, 366–379. [[CrossRef](#)]
13. Jing, J.; Lee, D.S.; Joe, J.; Kim, E.J.; Cho, Y.H.; Jo, J.H. A sensing-based visualization method for representing pressure distribution in a multi-zone building by floor. *Sensors* **2023**, *23*, 4116. [[CrossRef](#)] [[PubMed](#)]
14. Tamura, G.T.; Wilson, A.G. Pressure differences caused by chimney effect in three high buildings. *ASHRAE Trans.* **1967**, *73*, 1–10.
15. Park, S.-Y.; Lee, D.-S.; Ji, K.-H.; Jo, J.-H. Simplified model for estimating the neutral pressure level in the elevator shaft of a building. *Build Eng* **2023**, *79*, 107850. [[CrossRef](#)]
16. Xie, M.X.; Wang, J. Determination of Pressure Difference Coefficient of Shuttle Elevator Doors in Super High-Rise Buildings under Stack Effect. *Build. Environ.* **2023**, *232*, 110076. [[CrossRef](#)]
17. Shin, H.K. A Calculation Method for Determining Air Infiltration of High-Rise Buildings Based on Airtightness and Stack Effect Pressure. Ph.D. Thesis, Inha University, Incheon, Republic of Korea, 2018.

18. Walker, I.S.; Wilson, D.J. Evaluating models for superposition of wind and stack effect in air infiltration. *Build. Environ.* **1993**, *28*, 201–210. [[CrossRef](#)]
19. Jae-Hun, J.; Jae-Han, L.; Seung-Yeong, S.; Myoung-Souk, Y.; Kwang-Woo, K. Characteristics of pressure distribution and solution to the problems caused by stack effect in high-rise residential buildings. *Build. Environ.* **2007**, *42*, 263–277.
20. Hyunwoo, L.; Jungmin, S.; Doosam, S.; Sungmin, Y.; Joowook, K. Interaction analysis of countermeasures for the stack effect in a high-rise office building. *Build. Environ.* **2020**, *168*, 106530.
21. Khoukhi, M.; Hiroshi, Y.; Jing, L. The effect of the wind speed velocity on the stack pressure in medium-rise buildings in cold region of China. *Build. Environ.* **2007**, *42*, 1081–1088. [[CrossRef](#)]
22. Gang, T.; Leon, R.G. Application of integrating multi-zone model with CFD simulation to natural ventilation prediction. *Energy Build.* **2005**, *37*, 1049–1057.
23. Marcello, C.; Pascal, S.; Dominique, M. Full scale experimental study of single-sided ventilation: Analysis of stack and wind effects. *Ener. Build.* **2011**, *43*, 1765–1773.
24. Joonghoon, L.; Taeyon, H.; Doosam, S.; Jeong, T.K. Quantitative reduction method of draft in high-rise buildings, using revolving doors. *Indoor Built Environ.* **2012**, *21*, 79–91.
25. Joonghoon, L.; Beomseok, G.; Taeyon, H. Characteristics of revolving door use as a countermeasure to the stack effect in buildings. *J. Asian Architect. Build. Eng.* **2018**, *16*, 417–424.
26. Sung-Han, K.; Jae-Hun, J.; Hoi-Soo, S.; Myong-Souk, Y.; Kwang-Woo, K. Influence of architectural elements on stack effects in tall residential building. In Proceedings of the CTBUH 2004 Seoul Conference, Seoul, Republic of Korea, 10–13 October 2004.
27. Jungyeon, Y.; Angie, K.; Sanghwan, B.; Dongwoo, C.; Kee, H.K. HVAC operation schemes and commissioning process resolving stack effect problem and adjusting according to changes in the environment: A case study in high-rise building in South Korea. *Energies* **2021**, *14*, 2299.
28. Mengxiao, X.; Jian, W.; Jing, Z.; Jun, G.; Chengwei, P.; Chenyu, L. Field measurement and coupled simulation for the shuttle elevator shaft cooling system in super high-rise buildings. *Build. Environ.* **2021**, *187*, 107387.
29. Feustel, H.E. COMIS—An international multizone air-flow and contaminant transport model. *Energy Build.* **1999**, *30*, 3–18.
30. Khoukhi, M. A simplified procedure to investigate airflow patterns inside tall buildings using COMIS. *Archit. Sci. Rev.* **2007**, *50*, 365–369.
31. Wang, L.Z.; Chen, Q.Y. Evaluation of some assumptions used in multizone airflow network models. *Build. Environ.* **2008**, *43*, 1671–1677. [[CrossRef](#)]
32. Yoon, S.M.; Seo, J.M.; Cho, W.H.; Song, D.S. A calibration method for whole-building airflow simulation in high-rise residential buildings. *Build. Environ.* **2015**, *85*, 253–262. [[CrossRef](#)]
33. GB50009-2012; Load Code for the Design of Building Structures. Ministry of Housing and Urban-Rural Development of the People’s Republic of China (MOHURD): Beijing, China, 2012.
34. GB 50736-2012; Design Code for Heating Ventilation and Air Conditioning of Civil Buildings. Ministry of Housing and Urban-Rural Development of the People’s Republic of China (MOHURD): Beijing, China, 2012.
35. GB/T7106-2019; Test Methods of Air Permeability, Watertightness, Wind Load Resistance Performance for Building External Windows and Doors. Ministry of Housing and Urban-Rural Development of the People’s Republic of China (MOHURD): Beijing, China, 2019.
36. Tamblyn, R.T. Coping with air pressure problems in tall buildings. *ASHRAE Trans.* **1991**, *97*, 824–827.
37. Saroglou, T.; Theodosiou, T.; Givoni, B.; Meir, I.A. Studies on the optimum double-skin curtain wall design for high-rise buildings in the Mediterranean climate. *Ener. Build.* **2020**, *208*, 109641. [[CrossRef](#)]
38. Becker, R. Air Leakage of Curtain Walls—Diagnostics and Remediation. *Build. Phys.* **2010**, *34*, 57–75. [[CrossRef](#)]
39. Tamblyn, R.T. HVAC system effects for tall buildings. *ASHRAE Trans.* **1993**, *99*, 789–792.
40. Lovatt, J.E.; Wilson, A.G. Stack effect in tall buildings. *ASHRAE Trans.* **1994**, *100*, 420–431.

Disclaimer/Publisher’s Note: The statements, opinions and data contained in all publications are solely those of the individual author(s) and contributor(s) and not of MDPI and/or the editor(s). MDPI and/or the editor(s) disclaim responsibility for any injury to people or property resulting from any ideas, methods, instructions or products referred to in the content.